Geophys. J. Int. (2006) **166,** 782–794 doi: 10.1111/j.1365-246X.2006.03046.x

Spatial distribution of scatterers in the crust by inversion analysis of coda envelopes: a case study of Gauribidanur seismic array (Southern India)

A. Ugalde,[1] E. Carcolé[1] and J. N. Tripathi[2]

[1]*Ebro Observatory, CSIC – URL, Observatori de l'Ebre, Horta Alta* 38, 43520 *Roquetes, Tarragona, Spain. E-mail: augalde@obsebre.es*
[2]*Department of Earth and Planetary Sciences, University of Allahabad, Allahabad—*211002*, India*

Accepted 2006 April 21. Received 2006 February 15; in original form 2005 August 4

SUMMARY

The 3-D spatial distribution of relative scattering coefficients in southern India was estimated by means of an inversion technique applied to coda wave envelopes. The inversion analysis was performed for the first time in this kind of seismological research by means of the simultaneous iterative reconstruction technique and filtered backprojection method. Whereas the first one allows to obtain more exact solutions, the second one is a much faster non-iterative algorithm that has proved to provide very accurate reconstructions. Data used consisted of selected 636 vertical-component, short-period recordings of microearthquake codas from shallow earthquakes with magnitudes ranging from 0.7 to 3.7 and epicentral distances up to 120 km recorded by the Gauribidanur seismic array (GBA). Results are almost independent of the inversion method used and they are frequency dependent. They show a remarkably uniform distribution of the scattering strength in the crust around GBA. However, a shallow (0–24 km) strong scattering structure, which is only visible at low frequencies, seems to coincide with the Closepet granitic batholith which is the boundary between the eastern and western parts of the Dharwar craton.

Key words: crustal heterogeneity, inversion analysis, scattering coefficient, seismic coda, southern India.

1 INTRODUCTION

The behaviour of coda waves in seismograms is one of the observations supporting the existence of small-scale random heterogeneities in the Earth (Aki 1969; Aki & Chouet 1975; Sato *et al.* 2002). The direct *S* wave observed in a seismogram from a local earthquake is followed by complex wave trains with amplitudes smaller than the direct wave and that exponentially decay with time, which are called *S*-coda. It is widely accepted that coda waves are formed by superposition of incoherent scattered waves from randomly distributed heterogeneities in the lithosphere, such as cracks, faults, folds, and velocity or density anomalies with scale length about the seismic wavelength. *S*-coda waves have an envelope shape common to all epicentres and stations in a given region after twice the *S* wave traveltime (Rautian & Khalturin 1978). Total scattering coefficient (g) and coda attenuation (Q_c^{-1}) are the parameters, which characterize the coda excitation (which measures the capacity of the medium to originate scattering) and the decay rate of coda envelopes (which is a measure of the attenuation of the medium) within a given frequency band, respectively.

A number of models have been proposed to relate scattering and coda wave amplitudes. One approach to model the coda envelopes is to consider the heterogeneities as randomly and uniformly distributed point-like scatterers. Using this model and on the basis of the energy transport (or radiative transfer) theory (Wu 1985), the *S*-wave coda has been synthesized under the assumption of single isotropic scattering (SIS) (Sato 1977), multiple isotropic scattering (Hoshiba 1991; Zeng *et al.* 1991) and multiple non-isotropic scattering (Hoshiba 1995; Sato 1995).

On the other hand, scattering from randomly and non-uniformly distributed heterogeneities has also been studied to explain the features of the observed envelopes of *S* coda waves. Nishigami (1991) developed an inversion method of coda waveforms from local earthquakes to estimate the inhomogeneous spatial distribution of relative scattering coefficients in the crust. The method is based on the assumption that the fluctuation of the decay curve of the observed coda envelope from a reference curve, which was estimated by assuming SIS and spherical radiation from the source, is caused by a non-uniform distribution of scatterers in the crust. This method has proved to be an effective approach to investigate the real heterogeneous structure in the crust of several regions in the world: Nishigami (1991) detected zones of strong scattering related to major active faults in central Japan; Nishigami (1997) revealed significant heterogeneous structures in the crust around one active fault system and two active volcanoes in central Japan; and Nishigami (2000) showed the segmentation structure along the San Andreas fault system in

central California. Chen & Long (2000), in the Piedmont Province of central Georgia, found a correlation at shallow depths between zones of strong scattering and the location of hypocentres and areas with greater topographic relief, and were able to identify a strong reflecting layer which was consistent with a thrust plain previously reported using other geophysical methods. More recently, Asano & Hasegawa (2004) suggested the correlation between large scattering zones with the existence of fault-damaged zones in southwestern Japan, as well as other scattering properties of the region at different depths.

Several inversion methods have been used in order to obtain the strength of the scattering coefficients. Whereas Nishigami (1991) solved the problem using a standard inversion method, Nishigami (1997, 2000) used a recursive stochastic inversion method, and Chen & Long (2000) solved the inversion problem using the algebraic reconstruction technique (ART). On the other hand, Asano & Hasegawa (2004) revised the inversion analysis and obtained absolute values of the scattering coefficients by considering a depth dependent velocity structure and double-couple sources, and assuming an intrinsic absorption parameter.

The aim of this paper is to perform a coda envelope inversion analysis to microearthquake recordings by the Gauribidanur seismic array (GBA) to estimate a 3-D distribution of relative scattering coefficients in southern India. We will follow the method presented by Nishigami (1991). This method implies a previous knowledge of the depth dependent velocity model and it assumes a synthetic SIS model for the absolute reference scattering coefficients (Sato 1977). The observed data will be inverted using two different algorithms that are commonly used in biomedical applications but that have not been used previously in this kind of seismological applications: the simultaneous iterative reconstruction technique (SIRT) and the filtered backprojection (FBP) method. The first one allows to obtain better reconstructions than other inversion algorithms, however, it is slower. On the other hand, the FBP is a non-iterative method that has proved to provide fast and accurate solutions.

2 METHODS

2.1 The observation equation

Sometimes, the observed envelopes of *S* coda waves differ from those synthesized by models based on the hypothesis of uniform distribution of scatterers (e.g. Aki & Chouet 1975; Sato 1977). Small amplitude fluctuations or ripples overlying on a smoothly decaying coda envelope which is predicted by the scattering theory, are often observed. This observed behaviour can be explained by a non-uniform 3-D distribution of scatterers in the crust. Following Nishigami (1991), the structures causing strong scattering can be identified by analysing the observed coda envelope fluctuations from a synthesized (or reference) model.

In the present study we will consider the SIS approximation as the theoretical model for the absolute reference scattering coefficients. It models the shape of the coda of local earthquakes (Sato 1977) by assuming SIS, random and homogeneous distribution of scatterers in a constant velocity medium, and spherical radiation of elastic energy. According to the SIS model, and considering the anelastic attenuation effect, the coda energy density at a frequency f, hypocentral distance r and lapse time t in a 3-D space can be expressed as an integral all over the space in the form (Sato 1977):

$$E_s(f|r,t) = \int_V \frac{W_0(f) g(f)}{(4\pi)^2\, \beta\, r_1^2 r_2^2}\, \mathrm{e}^{-2Q_c^{-1}\pi f t}\, \delta\left[t - \frac{r_1 + r_2}{\beta}\right] dV, \quad (1)$$

where $dV = d^3x$; $\mathbf{x}$ is the coordinate vector of the scattering point; $r_1 = |\mathbf{x}|$ is the distance between the hypocentre and the scatterer; $r_2 = |\mathbf{x} - \mathbf{r}|$ is the distance between the scatterer and the station; $r = |\mathbf{r}|$; t is the lapse time measured from the origin time of the earthquake; β is the average *S*-wave velocity; $W_0(f)$ represents the total energy radiated from the source within a unit frequency band around f; and $g(f)$ is the total scattering coefficient for the frequency f. In a constant velocity medium, the scatterers responsible for the generation of coda waves at a distance r and time t are contained in a spheroidal shell whose foci are located at the source and receiver, which is expressed by the term $(1/\beta)\delta\,[t - (r_1 + r_2)/\beta]$ in eq. (1). Following Sato (1977) the integration of eq. (1) gives

$$E_s(f|r,t) = \frac{W_0(f)\, g_0(f)}{4\pi r^2}\, K(a)\, \mathrm{e}^{-2Q_c^{-1}\pi f t}, \quad (2)$$

for a homogeneous spatial distribution of the scattering coefficient $g_0(f)$, being $K(a) = (1/a)\ln\,[(a+1)/(a-1)]$ for $a > 1$; $a = t/t_S$; and t_S the *S*-wave traveltime. For $a \gg 1$ $K(a) \approx 2/a^2$, and therefore, eq. (2) becomes

$$E_s(f|r,t) \approx \frac{W_0(f)\, g_0(f)}{2\pi\beta^2 t^2}\, \mathrm{e}^{-2Q_c^{-1}\pi f t}, \quad (t > 2t_S), \quad (3)$$

which corresponds to the single scattering model of Aki & Chouet (1975).

We divide the volume under consideration into a number N of small blocks of volume δV, as it will be detailed later. Therefore, by multiplying the right side of eq. (1) by the factor 1/2 for including the effect of a half-space, then by integrating eq. (1) in the radial direction over the spheroidal shell (which radius is approximated by $\beta t/2$), which corresponds to the lapse time window $t_j \pm \delta t/2$, we obtain:

$$E_{sa}(f|t_j)\delta t \approx \frac{W_0(f)\, g_0(f)}{4\pi^2\beta t}\, \mathrm{e}^{-2Q_c^{-1}\pi f t_j} \sum_{i=1}^{N_j} \frac{\delta_{ij}}{(r_{1,i} r_{2,i})^2}\, \delta V, \quad (4)$$

where the integral has been approximated by a summation of the blocks, where each term corresponds to a certain block i. The sub index a in the energy density indicates the consideration of an average scattering coefficient g_0 over the half-space. δ_{ij} equals 1 when the ith block lays inside the spheroidal shell which corresponds to the j time window. N_j is the total number of scatterers in each spheroidal shell.

The observed coda envelope fluctuations from the theoretical model due to the non-uniform distribution of scatterers can be expressed mathematically as spatial perturbations of the average scattering coefficient of the medium due to an individual scatterer in the form: $g = g_0\ \alpha_i$ ($\alpha_i \geq 0$). Thus, the integration of eq. (1) gives

$$E_s(f|t_j)\delta t = \frac{W_0(f)\, g_0(f)}{4\pi^2\beta t}\, \mathrm{e}^{-2Q_c^{-1}\pi f t_j} \sum_{i=1}^{N_j i} \frac{\alpha_i \delta_{ij}}{(r_{1,i} r_{2,i})^2}\, \delta V. \quad (5)$$

For obtaining eqs (4) and (5) we have assumed a constant value of Q_c in the region (see Tripathi & Ugalde 2004 for an estimation of coda attenuation in the GBA region), thus neglecting the effect of an spatial variation of Q_c on the fluctuations of the coda envelope and considering that they are caused mainly by the spatial variations of the scattering coefficient. In order to get a system of equations that will allow us to estimate the spatial perturbations of the scattering coefficient we divide eq. (5) by eq. (4),

$$\frac{E_s(t_j)}{E_{sa}(t_j)} = \frac{1}{\sum_i \frac{\delta_{ij}}{(r_{1,i} r_{2,i})^2}} \sum_i \frac{\alpha_i \delta_{ij}}{(r_{1,i} r_{2,i})^2}, \quad (6)$$

where the left side of eq. (6) is called coda wave energy residual (e_j) and it measures the ratio of the observed energy density in this part of the coda to the average energy density of the medium.

If we divide the coda of one seismogram into several small time windows, we will have one equation based on eq. (6) for each time window. Also for each time window, the scatterers contributing to the energy density are contained in a spheroidal shell. Thus, eq. (6) can be rewritten in the following form

$$\begin{aligned} &w_{11}\alpha_1 + \cdots + w_{i1}\alpha_i + \cdots + w_{N1}\alpha_N = e_1 \\ &\qquad\qquad \vdots \\ &w_{1j}\alpha_1 + \cdots + w_{ij}\alpha_i + \cdots + w_{Nj}\alpha_N = e_j, \\ &\qquad\qquad \vdots \\ &w_{1M}\alpha_1 + \cdots + w_{iM}\alpha_i + \cdots + w_{NM}\alpha_N = e_M \end{aligned} \tag{7}$$

where M is the total number of equations (number of seismograms multiplied by the number of coda time windows considered), N is the total number of scatterers (number of small blocks into which the study region is divided) and

$$w_{ij} = \frac{1}{\sum_i \frac{\delta_{ij}}{(r_{1,i}r_{2,i})^2}} \frac{\delta_{ij}}{(r_{1,i}r_{2,i})^2}. \tag{8}$$

2.2 The inversion methods (SIRT and FBP)

To solve systems of equations as large as eq. (7) there exist some powerful iterative methods (e.g. Kak & Slaney 1988). These methods were first successfully used in tomographic imaging for medical applications and have been extended to other scientific fields. The simplest iterative method is the so-called ART algorithm. For the use of this method it is necessary to make an arbitrary initial guess of the solution $\vec{\alpha}^0 = (\alpha_1^0, \alpha_2^0, \cdots, \alpha_N^0)$. In our case we simply assign a unity value to all the α_j^0 . Then the ART iteration process can be mathematically described by the following equation:

$$\Delta\alpha_j^{(i)} = \alpha_j^{(i)} - \alpha_j^{(i-1)} = \frac{\vec{\alpha}^{(i-1)} \cdot \vec{w}_i - e_i}{\vec{w}_i \cdot \vec{w}_i}, \tag{9}$$

where $\vec{w}_i = (w_{i1}, w_{i2}, \cdots, w_{iN})$, and the next solution $\alpha_j^{(i)}$ is changed from the preceding one $\alpha_j^{(i-1)}$ by the addition of the quantity $\Delta\,\alpha_j^{(i)}$. This method was applied by Chen & Long (2000) to solve a similar problem.

However, ART reconstructions usually suffer from 'salt and pepper' noise which is caused by the inconsistencies introduced in the set of equations by the approximations commonly used in the calculation of the matrix parameters. The SIRT (Kak & Slaney 1988) is another algorithm which eliminates the continual and competing block update as each equation is considered. Then, by using the SIRT algorithm, smoother and better-looking reconstructions are usually obtained at the expense of slower convergence. It is also known that SIRT algorithms perform better in extreme situations such as uneven distribution of data, incompleteness, etc., and it is also possible to easily incorporate constrains as positivity and limited spatial support. The SIRT algorithm computes the correction for each block at each iteration by the use of the same equations as in the ART algorithm, but before making any changes, all the equations are considered and only at the end of each iteration the block values are updated. The correction applied to each block is then the average value of all the computed changes for that block.

In many ART and SIRT implementations the w_{ij}'s are simply replaced by 1's and 0's depending on whether the centre of the ith block is within the jth spheroidal shell. However, the width of the shell is usually smaller than the width of the block. Thus, in our case, in order to perform a more accurate inversion, we approximately evaluate the fraction of volume V_{ij} of each block lying inside the jth spheroidal shell. In this way we prevent the overestimation or underestimation that occurs when only 1's and 0's are considered. Thus, we rewrite the coefficients w_{ij} as:

$$w_{ij} = \frac{1}{\sum_i \frac{V_{ij}}{(r_{1,i}r_{2,i})^2}} \cdot \frac{V_{ij}}{(r_{1,i}r_{2,i})^2}. \tag{10}$$

It is also important to use a relaxation (or smoothing) parameter λ (a factor smaller than unity multiplying the correction factor). If incorrectly selected, it will either cause premature termination and incorrect result or, if the number of iterations or λ is too small, it will result in a reconstruction lacking high-frequency details. By trial and error we chose $\lambda \sim 0.01$ for about 120 iterations.

There are other faster non-iterative methods which provide solutions to this type of systems of equations. A very convenient and widely used method is the FBP algorithm (Kak & Slaney 1988). In this algorithm the scattering coefficients become simply a weighted average value of the residuals that correspond to a certain block. This makes FBP much faster than any other iterative method. Computation times are about 100 times smaller than the ones for ART or SIRT and no relaxation parameter has to be chosen. The correspondence between the scattering coefficients and the residuals are established following several steps:

(i) For each earthquake k, the traveltime of the signal from the source to the ith block plus the traveltime from the ith block to each seismograph l is computed. This time is named T_{ikl}. With this data we define the corresponding spheroidal surface S_{ikl}. The centre of the ith block lies on S_{ikl} and the foci correspond to the location of the hypocentre and the station. Note that each block defines a different spheroidal surface.

(ii) The corresponding magnitude of the residuals for each earthquake k and each station l at the time T_{ikl} is then computed by simple linear interpolation between two consecutive e_j, because the available discrete data is spaced δt. We call this magnitude $R(T_{ikl})$.

(iii) The contribution of each block is proportional to $1/(r_{1,i}\, r_{2,i})^2$. This factor indicates whether the contribution of a certain block is more or less important than the contribution of other blocks on the spheroidal surface S_{ikl}. Then the spatial perturbation of the scattering coefficient may be written as:

$$\alpha_i = \frac{\sum_k \sum_l w_{ikl} R(T_{ikl})}{\sum_k \sum_l w_{ikl}}. \tag{11}$$

Note that each weight in eq. (11) corresponds to a different spheroidal surface. In order to normalize the contribution of the weights for each spheroidal surface we consider that a good definition for the weights would be:

$$w_{ikl} = \frac{(1/r_{1,i})^2 (1/r_{2,i})^2}{\left\langle (1/r_{1,i})^2 (1/r_{2,i})^2 \right\rangle_{S_{ikl}}}. \tag{12}$$

We think this definition is very convenient because an analytical expression can be written for the average value. In this way the weights only depend on the location of the ith block, the hypocentre and the station. This is an important point in order to perform a faster calculation. The average value can be written as:

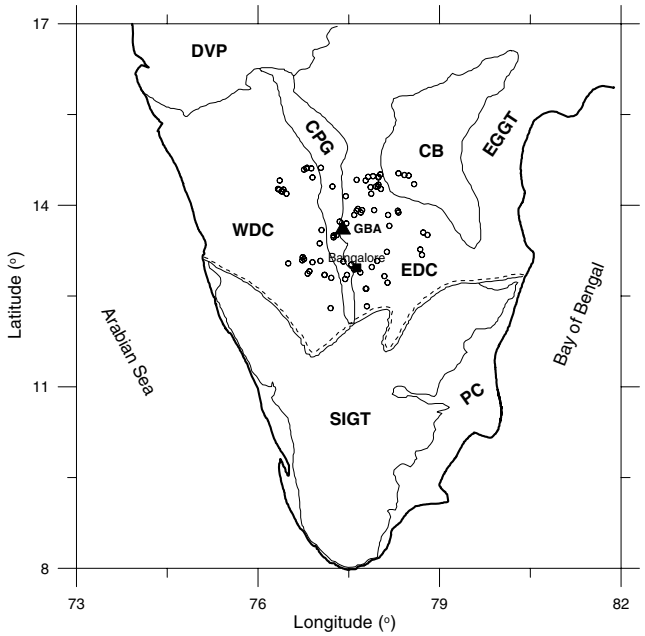

Figure 1. General geological sketch map of southern India. DVP, Deccan volcanic province; WDC, western Dharwar craton; EDC, eastern Dharwar craton; SIGT, south Indian granulite terrain; EGGT, eastern Ghat granulite terrain; CPG, closepet granite; CB, Cuddapah basin and PC, Phanerozoic sedimentary cover. Dotted line indicates Fermor's line (boundary between Dharwar craton and south India granulite terrain). The location of the epicentres used for the analysis is also shown (from Tripathi & Ugalde 2004).

$$\left\langle (1/r_{1,i})^2 (1/r_{2,i})^2 \right\rangle_{S_{ikl}} = \frac{1}{A_{ikl}} \int_{S_{ikl}} (1/r_{1,i})^2 (1/r_{2,i})^2 \, dS, \tag{13}$$

where A_{ikl} is the area of S_{ikl}. This integral is analogous to the one solved by Sato (1977). Thus, we may write:

$$\int_{S_{ikl}} (1/r_{1,i})^2 (1/r_{2,i})^2 \, dS = \frac{4\pi}{r\beta T_{ikl}} \cdot \ln\left(\frac{\beta T_{ikl} + r}{\beta T_{ikl} - r}\right). \tag{14}$$

By considering the expression for the area of a spheroid we may then write:

$$A_{ikl} = \frac{\pi}{2}\left(\beta^2 T_{ikl}^2 - r^2 + \beta^2 T_{ikl}^2 \frac{\sqrt{1-(r/\beta T_{ikl})^2}}{r/\beta T_{ikl}} \arcsin(r/\beta T_{ikl})\right). \tag{15}$$

And finally we obtain:

$$w_{ikl} = \frac{r\beta T_{ikl}}{8(r_{1,i} r_{2,i})^2} \frac{\left(\beta^2 T_{ikl}^2 - r^2 + \beta^2 T_{ikl}^2 \frac{\sqrt{1-(r/\beta T_{ikl})^2}}{r/\beta T_{ikl}} \arcsin(r/\beta T_{ikl})\right)}{\ln\left(\frac{\beta T_{ikl}+r}{\beta T_{ikl}-r}\right)}. \tag{16}$$

In this work, we compare the results of the application of the two inversion algorithms described. Additionally, some conclusions about the practical implementations of the methods are reached.

3 GEOLOGICAL SETTING AND DATA

The GBA is located in the Indian peninsula, about 90 km north of Bangalore, on the western flank of the eastern Dharwar craton which is one of the oldest geological provinces in southern India (Fig. 1). The region is divided into the western (which is composed of old gneisses and greenstones with very few granites) and eastern (which is made of younger rocks with widespread N–S elongate plutons of late Archaeani granites) parts by the 400 km long and 20–30 km wide, north–south trending granitic intrusion named Closepet batholith (Moyen *et al.* 2003). The area around the array is relatively flat, with a few hill ranges towards the east and the south. Thus, the topographic influence on scattering would be very small. A crustal model consisting of a 16 km thick top granitic layer over a second layer 19 km thick above the mantle (i.e. with the Moho at 35 km depth) was proposed by Arora (1971) and observed *S*-wave velocities were 3.46, 3.96 and 4.61 km s^{-1}, respectively.

Waveform data used were selected from 80 earthquakes with epicentral distances up to 120 km which were recorded by the GBA in the period 1992 January to 1995 December. GBA is an *L*-shaped seismic array and each arm contains 10 short-period ($T_0 =$ 1 s) vertical-component seismometers spaced at intervals of about 2.5 km. The recorded signals are digitized at a sampling interval of 0.05 s. All the events are shallow (depths less than 10 km) and local magnitudes range between 0.3 and 3.7. Attending to the quality of data and after a careful visual inspection, only 636 vertical-component, high-quality waveforms were finally processed.

4 DATA ANALYSIS AND RESULTS

One example of the analysis procedure (Nishigami 1991) is shown in Fig. 2. First, each seismogram was bandpass filtered over the

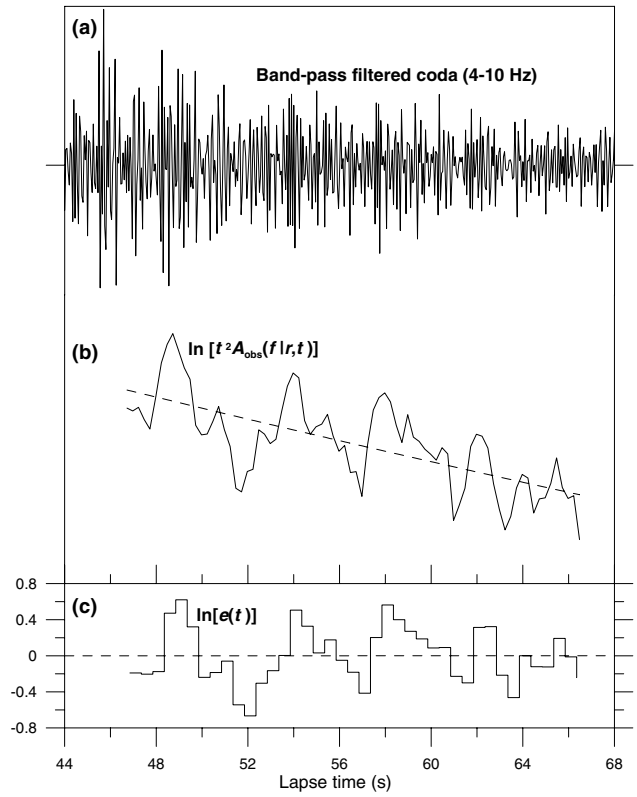

Figure 2. Example of the processing steps for obtaining the coda energy residuals: (a) bandpass filtered coda waveform of an earthquake at an epicentral distance of 90.6 km; (b) logarithm of the running mean-squared amplitudes corrected for geometrical spreading effect. The discontinuous line is the best linear fitting function to the logarithmic trace and (c) logarithm of the coda energy residuals averaged in a time window of 0.5 s.

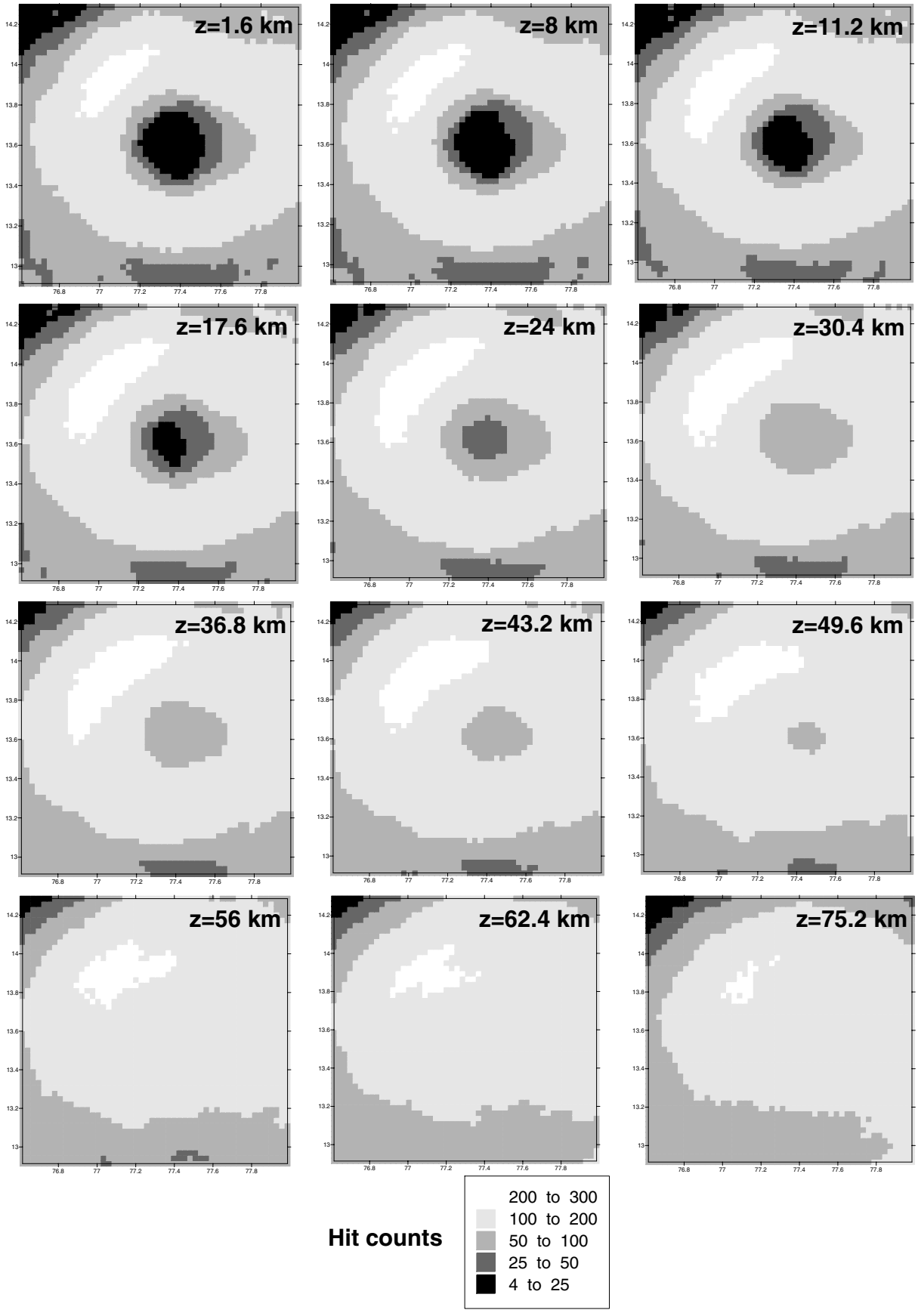

Figure 3. Hit counts or number of coda residuals contributed by each block. It measures the number of times each block is sampled by the scattering shells of observed coda data. The darker areas are the zones lesser sampled by the spherical shells.

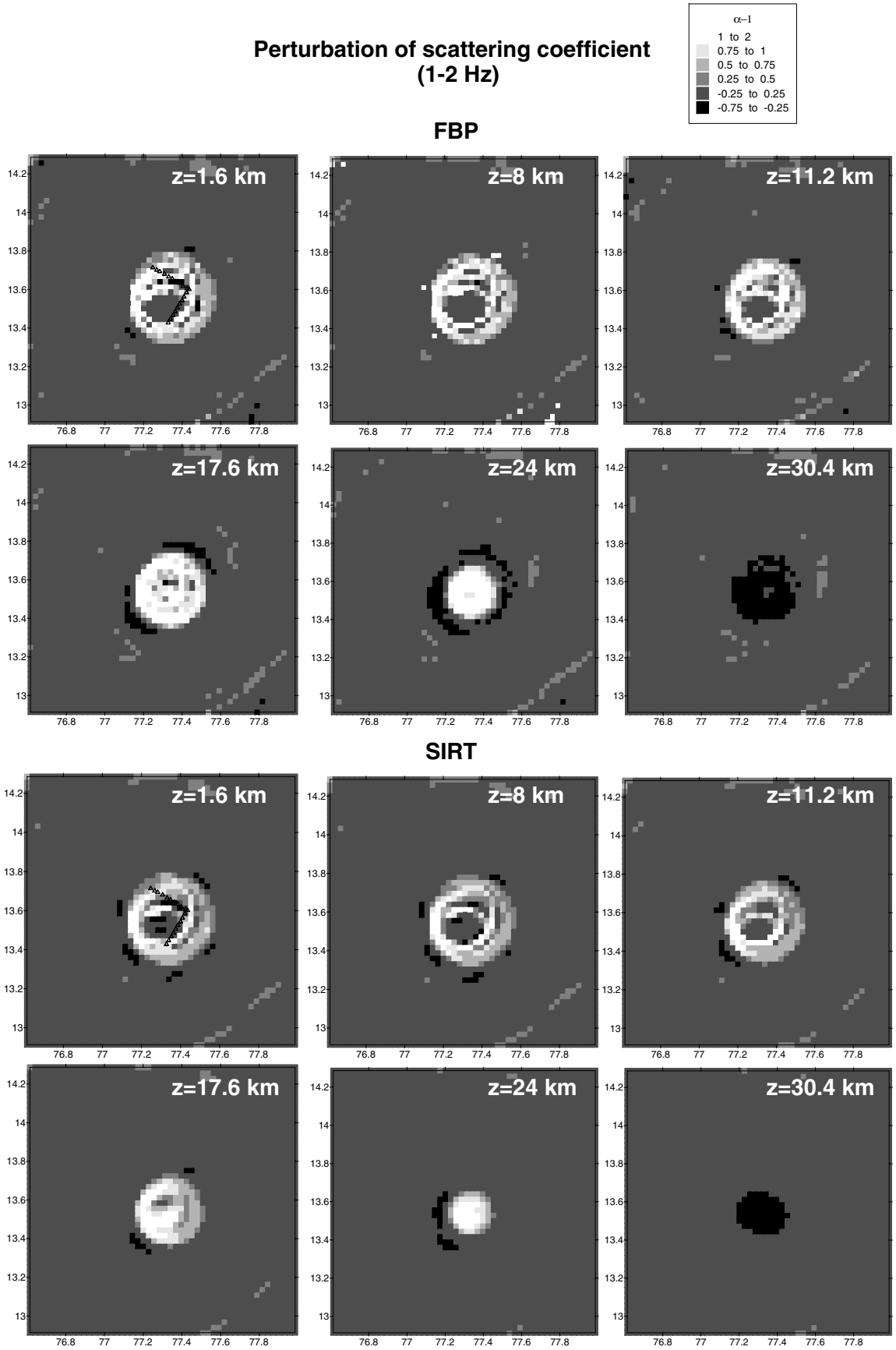

Figure 4. Spatial distribution of relative scattering coefficients for different depths and for the two inversion methods used: (a) results for the frequency band 1–2 Hz; (b) 2–4 Hz and (c) 4–10 Hz. The lightest zones indicate the strongest perturbations from an average scattering coefficient.

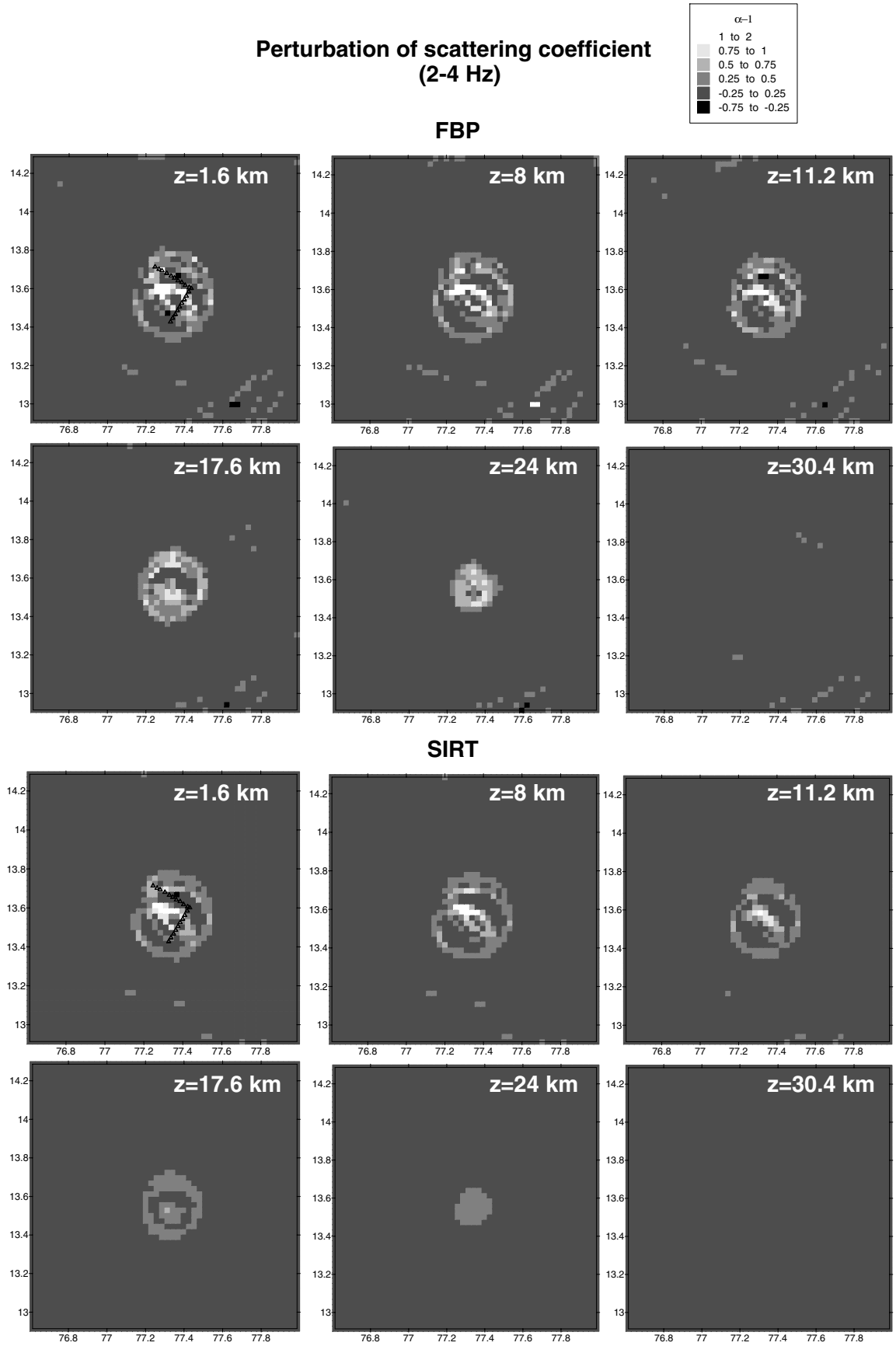

Figure 4. (*Continued.*)

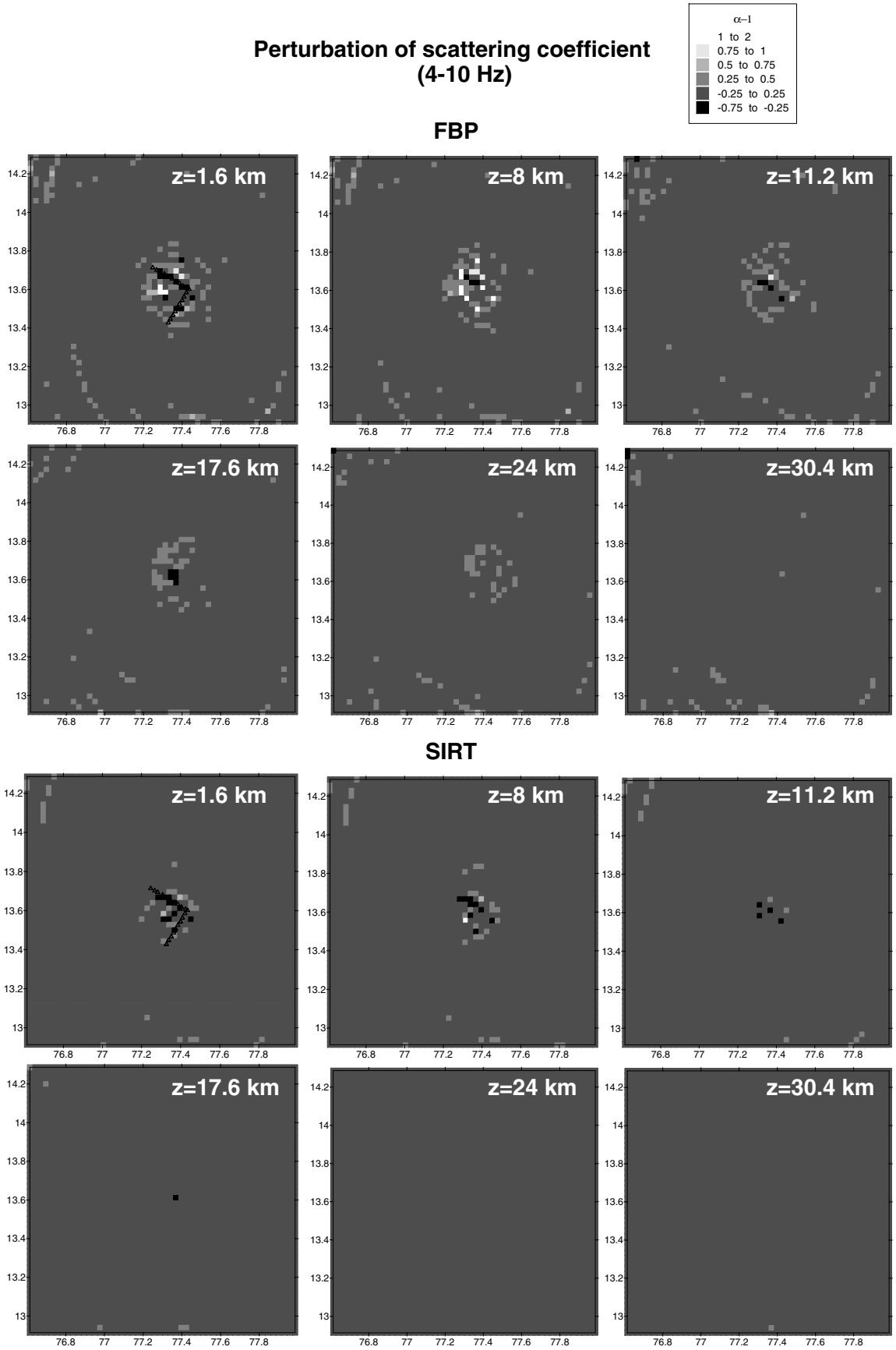

Figure 4. (*Continued.*)

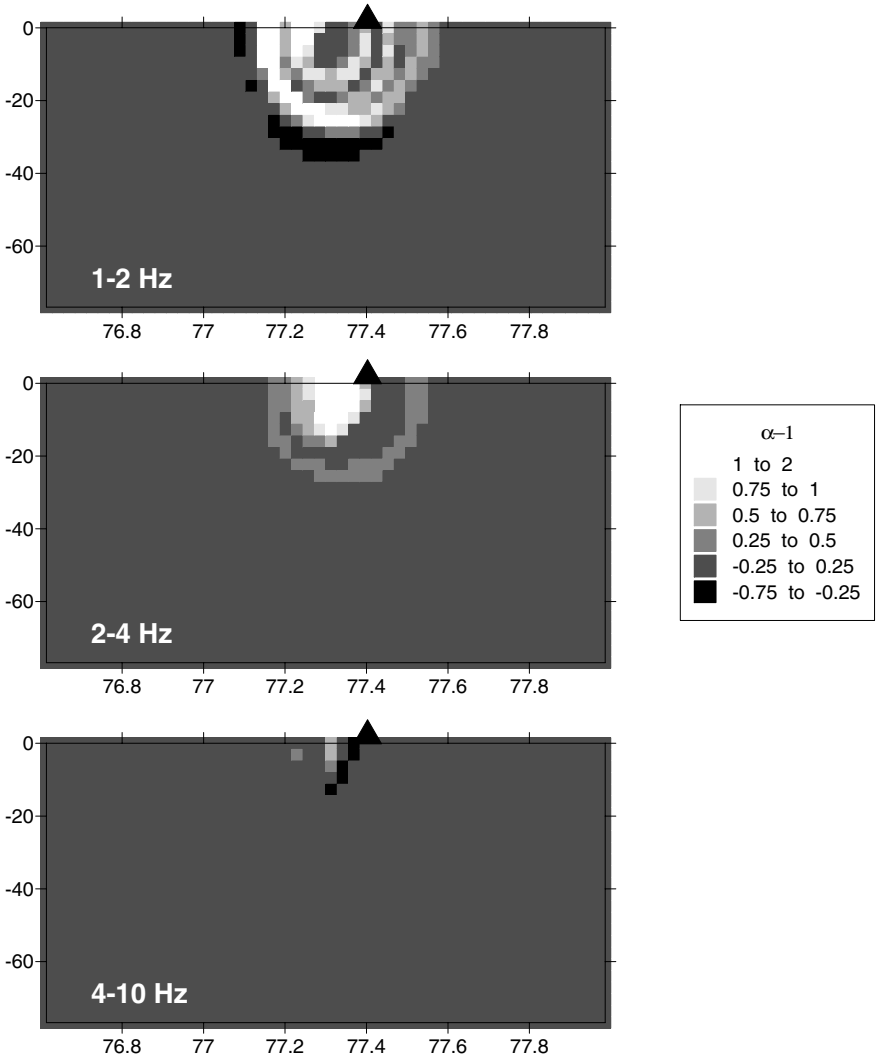

Figure 5. Vertical cross-section of relative scattering coefficients at the parallel 13.6°, which corresponds to the latitude of the array crosspoint.

frequency bands 1–2 (1.5 ± 0.5) Hz, 2–4 (3 ± 1) Hz and 4–10 (7 ± 3) Hz. Then, the rms amplitudes $A_{\rm obs}(f|r, t)$ were calculated by using a 0.25 s spaced moving time window of length $t \pm 2$ s, $t \pm 1$ s, and $t \pm 0.5$ s for the first, second and third frequency band, respectively. The time interval for the analysis started at 1.5 times the *S*-wave traveltimes (in order to increase the resolution near the source region) and had a maximum length of 20 s (to minimize the effects of multiple scattering). The rms amplitudes for a noise window of 10 s before the *P*-wave arrival were also computed and only the amplitudes greater than two times the signal to noise ratio were kept. The amplitudes were then corrected for geometrical spreading by multiplying by t^2 which is valid for body waves in a uniform medium. Then, the average decay curve was estimated for each seismogram by means of a least-squares regression of $\ln[t^2 A_{\rm obs}(f|r, t)]$ versus t and only the estimates with a correlation coefficient greater than 0.60 were kept. The observed coda residuals $e(t)$ were then calculated by taking the ratio of the corrected observed amplitudes to the estimated exponential decay curve. Finally the residuals were averaged in time windows of $\delta t = 0.5$ s to get e_j at discrete lapse times t_j. The decrease of δt increases the spatial resolution, but also the size of the inversion problem. In this case, the system (7) has a number of equations of ~2700 for the frequency bands centred at 1.5 and 7 Hz, and ~5200 equations for the 3 Hz centre frequency. The time window for the averaging must also satisfy the condition $\delta t \leq 2(\delta V)^{1/3}/\beta$, where δV is the volume of one small block into which the study area is divided and $\beta = 3.65$ km s^{-1} in this region (Arora 1971; Krishna & Ramesh 2000). This condition assures that the width of each spheroidal shell is smaller than the size of a block.

We selected a 155×155 km in horizontal and 80 km in depth study region attending to the stations and hypocentres distribution and it was divided into $N = 50 \times 50 \times 25$ blocks. Then, the observational system of eq. (7) was created by assuming the layered velocity structure by Arora (1971) and it was solved using the SIRT and FBP algorithms.

Before discussing the results, we examine the reliability of the solution. Fig. 3 shows the hit counts, or number of coda residuals contributed by each block, that shows which grid zones may be affected by sampling insufficiency for the grid defined. It can be observed that the entire region is sampled by the ellipses, however, the hit counts are much less in an area close around the array and they increase both in horizontal and depth directions up to the considered depth of 80 km. This happens because the stations are concentrated in a small area, which makes all the blocks which are close to the

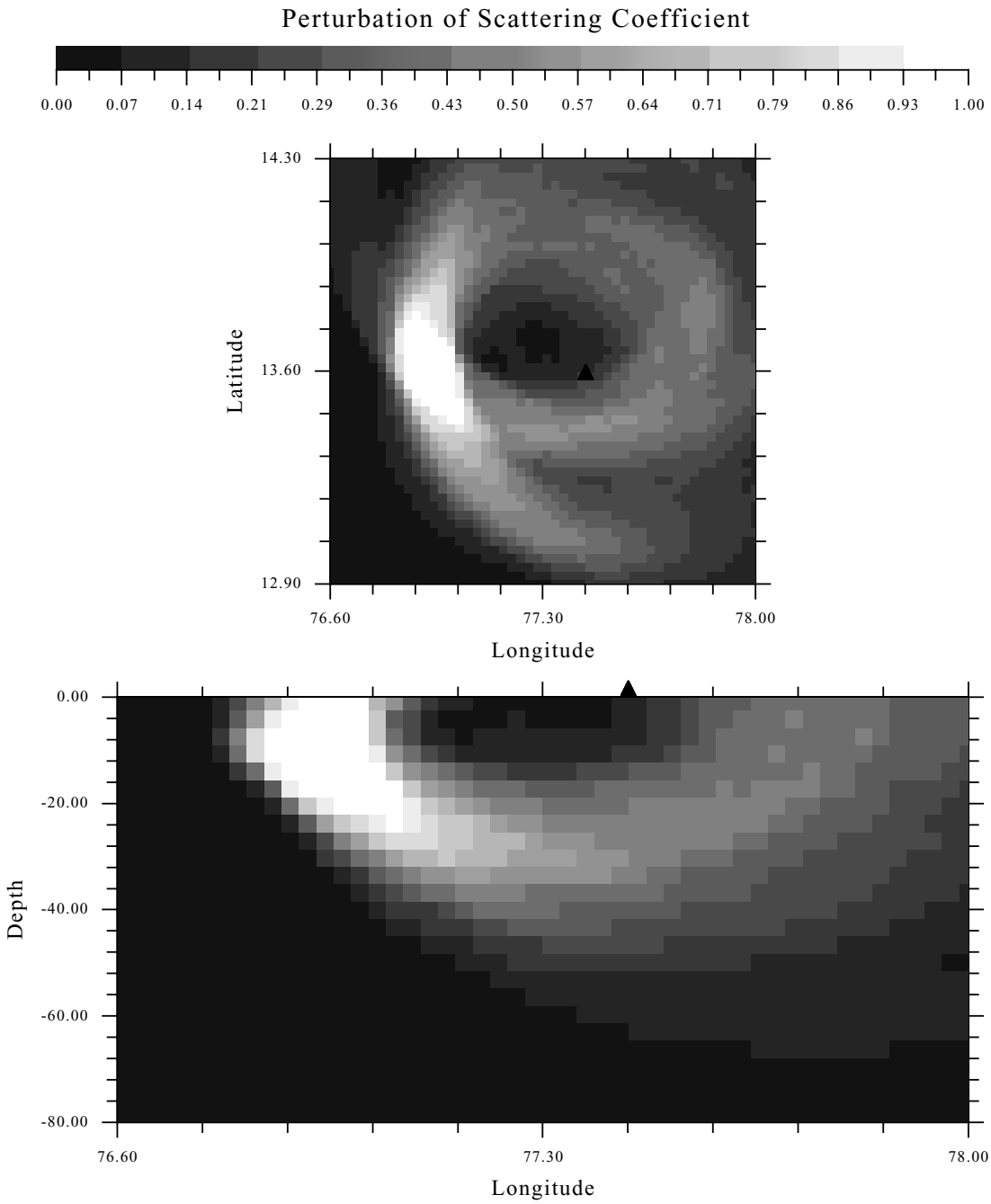

Figure 6. Spatial distribution of relative scattering coefficients for a synthetic test consisting of one spheroidal structure with two horizontal semi-axes of 13 km and the vertical semi-axis of 9.3 km. It was located at different distances from the array centre point, which is shown by a solid triangle: (a) to the west; (b) below and (c) to the east. The pattern recovered at a depth of 0 km is plotted at the top of the figure. The vertical cross-section along the plane defined by the latitude of the array centre point is also shown.

array to correspond to short lapse times, and they are few because we omitted the earliest portion of the *S*-wave coda by adopting $1.5t_S$ as start time for the analysis.

On the other hand, we tested the resolution of the inversion methods by synthesizing the coda energy residuals from the observational equation using a given test distribution of scattering coefficients and the same distribution of stations and events used in the analysis. We generated vertical structures with positive perturbations of the scattering coefficient with horizontal dimensions equal to one block and depths up to 80 km embedded in a non-perturbed medium. Then the synthesized residuals were inverted. Results show that although the vertical structures are seen almost up to the maximum depth considered of 80 km, they are well reproduced (more than 50 per cent of the perturbation value is returned) only up to the seventh block (22.4 km).

The resulting distribution of relative scattering coefficients $\alpha - 1 = (g - g_0)/g_0$ in the study region for the three analysed frequency bands and for different depths is plotted in Fig. 4. The lightest tones indicate scattering coefficients larger than the average in this region.

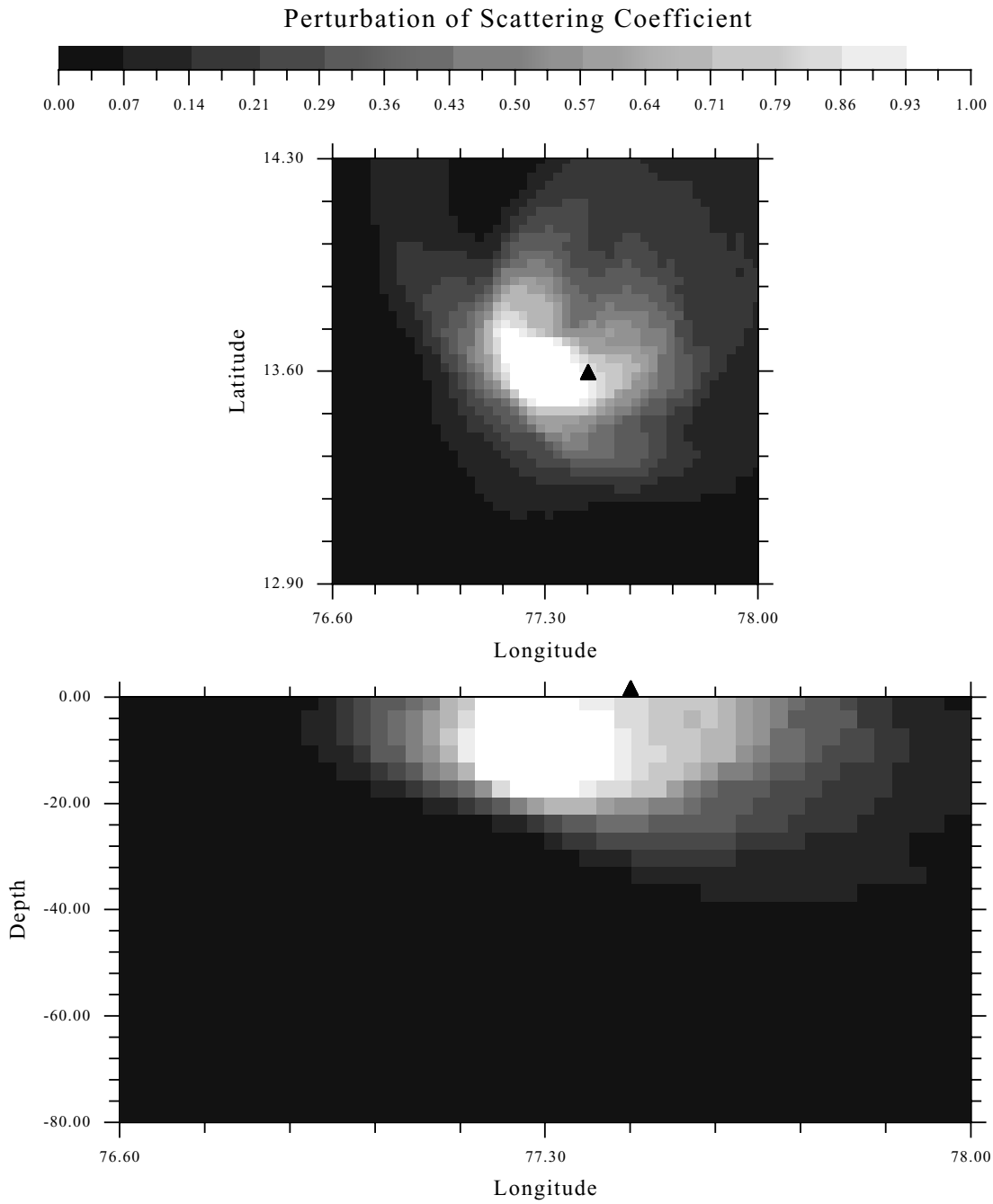

Figure 6. (*Continued.*)

5 DISCUSSION

It can be observed that we obtain practically the same distribution of relative scattering coefficients regardless of applying the SIRT or FBP inversion algorithms. Whereas the SIRT algorithm provides slightly lower values of the relative scattering coefficients, the FBP method provides more contrast. Thus, we would recommend the use of the FBP method, which requires much lesser (about 100 times) computation time.

On the other hand, Fig. 4 shows that more than the 90 per cent of the analysed region reveals a spatial perturbation of the scattering coefficient between ±25 per cent. This means that the crust around GBA presents a remarkably uniform distribution of scattering coefficients. For low frequencies, this uniformity is broken by the presence of a strong scattering area which is recognized from the surface up to a depth of 24 km just below the array. This structure is not observed at high frequencies. In fact, each analysed frequency band is giving us information about inhomogeneous structures with sizes comparable to the seismic wavelengths (∼1.8 to ∼3.6 km for 1–2 Hz, ∼900 m to ∼1.8 km for 2–4 Hz, and ∼360 m to ∼900 m for 4–10 Hz in this case). Fig. 5 shows a cross-section of relative scattering coefficients shown in Fig. 4 projected onto the vertical plane defined by the parallel of the array centre point. It can be observed that the strongest scatterers are located on the western part of GBA. However, Figs 4 and 5 show that the heterogeneity follows an ellipsoidal pattern. This may happen because this area is poorly sampled

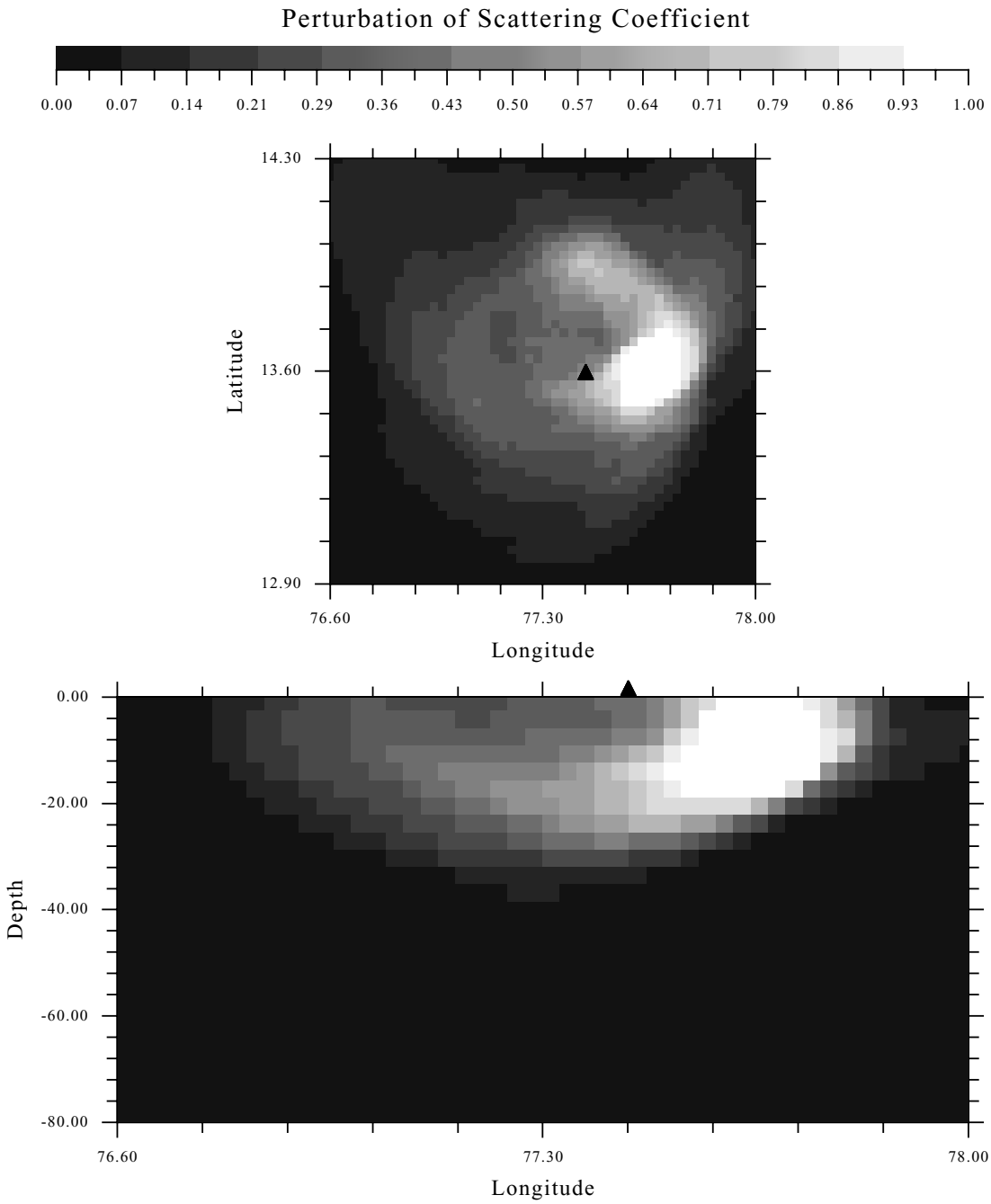

Figure 6. (*Continued.*)

by the ellipses as previously discussed in Fig. 3, however, the behaviour is only observed for the lowest frequency band analysed. In fact, we detected high values of the residuals at low frequencies and short lapse times. In order to establish the validity of the results of this study we tested the inversion method by means of a synthetic test. Because the most notable geological feature in the considered region is the 400 km long and 20–30 km wide, north–south trending Closepet granitic intrusion, we simulated the existence of a single spheroidal structure with positive perturbations of the scattering coefficient at different locations in a non-perturbed medium. Results of the inversion of the synthesized residuals are shown in Fig. 6. It can be observed that the patterns of the test are well reproduced. We may then conclude that the scattering region observed near the array centre point (Fig. 4) is neither a ghost image nor a mathematical artefact. Thus we may consider that the inversion method may reproduce up to a certain extent the observed data.

With respect to the uniform distribution of scattering coefficients, our results are in accordance with previous studies performed in the region. In an early work in this region using statistical analysis of observed teleseismic traveltime residuals, Berteussen *et al.* (1977) remarked that the area on which GBA is sited presents exceptionally homogeneous structures, apart from the general existing velocity perturbations of the order of a few percent. This conclusion was partly supported by Mohan & Rai (1992), who also detected the presence of a prominent scatterer in the deep crustal and uppermost mantle level (30–55 km) in this region from a

semblance technique analysis. The scattering region coincided with the Closepet granitic intrusion in the region. Krishna & Ramesh (2000) performed a frequency–wavenumber (f–k) spectral analysis of *P*-coda waveforms to mine tremors and explosions recorded at GBA array. They found a near-on azimuth dominant energy peak with apparent velocity appropriate to the upper crustal depths and they interpreted the result by the presence of a scattering waveguide at upper crustal depths (5–15 km) which might be also related to the granitic batholith. In our case, the zone of strong relative scattering coefficients at low frequency to the west of the GBA array cross-point also coincides with the so-called Closepet batholith, which is a granitic intrusion that acts as the major geological boundary in the region and it is believed to be a Precambrian suture zone between the eastern and western Dharwar craton.

6 CONCLUSIONS

We estimated the 3-D distribution of relative scattering coefficients in the crust in southern India by means of an *S*-wave coda envelope inversion technique applied to local recordings by the GBA. Two different inversion algorithms were used for the first time in this type of seismological research: the SIRT and the FBP method. The results allowed us to reach the following conclusions:

(1) The spatial distribution of the relative scattering coefficients obtained was almost independent of the inversion method used.

(2) The FBP method is very convenient and appropriate for solving these kinds of problems because it requires about 100 times less computation time than the SIRT algorithm to invert the data.

(3) The crust of the analysed region around GBA showed a remarkably uniform distribution of scatterers at more than the 90 per cent of the area, which is in accordance with the conclusions of previous studies in the region using statistical analysis of observed teleseismic traveltime residuals.

(4) An inhomogeneous structure with size comparable to a wavelength of ∼1.8 to ∼3.6 km for 1.5 Hz was detected to the west of GBA from the surface up to a depth of about 24 km just below the array and it coincides with the Closepet granitic intrusion which is the major geological boundary between the eastern and western Dharwar craton.

ACKNOWLEDGMENTS

The authors are very grateful to the GBA authorities and staff for providing the data used in this study. We also acknowledge useful comments and suggestions by H. Sato, L. T. Long and Y. Asano. The editor A. Curtis, J. Spetzler and an anonymous reviewer provided helpful comments which improved the manuscript.

REFERENCES

Aki, K., 1969. Analysis of the seismic coda of local earthquakes as scattered waves, *J. geophys. Res.,* **74,** 615–631.

Aki, K. & Chouet, B., 1975. Origin of coda waves: source, attenuation and scattering effects, *J. geophys. Res.,* **80,** 3322–3342.

Arora, S.K., 1971. A study of the earth's crust near Gauribidanur, South India, *Bull. seism. Soc. Am.,* **61,** 671–683.

Asano, Y. & Hasegawa, A., 2004. Imaging the fault zones of the 2000 western Tottori earthquake by a new inversion method to estimate three-dimensional distribution of the scattering coefficient, *J. geophys. Res.,* **109,** B06306, doi:10.1029/2003JB002761.

Berteussen, K.A., Husebye, E.S., Mereu, R.F. & Ram, A., 1977. Quantitative assessment of the crust-upper mantle heterogeneities beneath the Gauribidanur seismic array in southern India, *Earth Planet. Sci. Lett.,* **37,** 326–332.

Chen, X. & Long, L.T., 2000. Spatial distribution of relative scattering coefficients determined from microearthquake coda, *Bull. seism. Soc. Am.,* **90,** 512–524.

Hoshiba, M., 1991. Simulation of multiple scattered coda wave excitation based on the energy conservation law, *Phys. Earth planet. Int.,* **67,** 123–136.

Hoshiba, M., 1995. Estimation of nonisotropic scattering in western Japan using coda wave envelopes: application to a multiple nonisotropic scattering model, *J. geophys. Res.,* **100,** 645–657.

Kak, A.C. & Slaney, M., 1988. *Principles of Computerized Tomographic Imaging*, IEEE Press, New York.

Krishna, V.G. & Ramesh, D.S., 2000. Propagation of crustal-waveguide-trapped Pg and seismic velocity structure in South Indian shield, *Bull. seism. Soc. Am.,* **90,** 1281–1294.

Mohan, G. & Rai, S.S., 1992. Imaging of seismic scatterers beneath the Gauribidanur (GBA) array, *Phys. Earth Planet. Int.,* **71,** 36–45.

Moyen, J.F., Nédélec, A., Martin, H. & Jayananda, M., 2003. Syntectonic granite emplacement at different structural levels : the Closepet granite, South India, *J. Struc. Geol.,* **25,** 611–631.

Nishigami, K., 1991. A new inversion method of coda waveforms to determine spatial distribution of coda scatterers in the crust and uppermost mantle, *Geophys. Res. Lett.,* **18,** 2225–2228.

Nishigami, K., 1997. Spatial distribution of coda scatterers in the crust around two active volcanoes and one active fault system in central Japan: Inversion analysis of coda envelope, *Phys. Earth planet. Int.,* **104,** 75–89.

Nishigami, K., 2000. Deep crustal heterogeneity along and around the San Andreas fault system in central California and its relation to segmentation, *J. geophys. Res.,* **105,** 7983–7998.

Pulli, J.J., 1984. Attenuation of coda waves in New England, *Bull. seism. Soc. Am.,* **74,** 1149–1166.

Rautian, T.G. & Khalturin, V.I., 1978. The use of coda for determination of the earthquake source spectrum, *Bull. seism. Soc. Am.,* **68,** 923–948.

Sato, H., 1977. Energy propagation including scattering effects; single isotropic scattering, *J. Phys. Earth,* **25,** 27–41.

Sato, H., 1995. Formulation of the multiple non-isotropic scattering process in 3-D space on the basis of the energy transport theory, *Geophys. J. Int.,* **121,** 523–531.

Sato, H., Fehler, M. & Wu, R.-S., 2002. Scattering and attenuation of seismic waves in the lithosphere, Chapter 13 in *International Handbook of Earthquake and Engineering Seismology*, pp. 195–208, eds Jennings, P., Kanamori, H. & Lee, W.

Tripathi, J.N. & Ugalde, A., 2004. Regional estimation of *Q* from seismic coda observations by the Gauribidanur seismic array (southern India), *Phys. Earth planet. Int.,* **145,** 115–126.

Wu, R.-S., 1985. Multiple scattering and energy transfer of seismic waves—separation of scattering effect from intrinsic attenuation—I. Theoretical modelling, *Geophys. J. R. astr. Soc.,* **82,** 57–80.

Zeng, Y., Su, F. & Aki, K., 1991. Scattered wave energy propagation in a random isotropic scattering medium, I, Theory, *J. geophys. Res.,* **96,** 607–619.